13th September 2024

$B^0 \to K^* \ell^+ \ell^-$

Alice De Vito [1]

University of Milan–Bicocca
CERN Summer Student 2024

Supervisors:
Marcella Bona and Marzia Bordone

Abstract

This study investigates the rare decay $B \to K^* \ell^+ \ell^-$, a process sensitive to new physics. We compute the branching ratios for $\ell = \mu$, e, incorporating state-of-the-art form factors and uncertainties. Our predictions are compared with LHCb experimental results, revealing a notable discrepancy quantified through the Wilson coefficient C_9.

Using 2018 ATLAS data, we extract the S-wave fraction of the $K\pi$ system in the decay $B^0 \to K^*(892) J/\psi(\to e^+ e^-)$. This work underscores the complexity of this decay and their potential for probing new physics, while highlighting the importance of considering the $K\pi$ system's intricate dynamics in future rare B-meson decay analyses.

[1] a.devito7@campus.unimib.it

1 Introduction

In the Standard Model (SM), the weak charged current is the only flavour-violating interaction. The probability of changes between the quarks flavours is controlled by the Cabibbo-Kobayashi-Maskawa (CKM) mixing matrix, that is almost flavour diagonal. Flavour-Changing-Neutral-Current (FCNC) processes, which involve the transformation of a quark into another one of the same type but with a different flavour, are suppressed by the Glashow-Iliopoulos-Maiani mechanism and require at least one off-diagonal element in the CKM matrix. Hence, these processes are forbidden at tree level making them rare. The FCNC transitions $b \to s$ are among the most valuable probes of flavour physics and they are highly sensitive to new physics(NP): if new heavy particles exist, they could contribute to FCNC decay amplitudes and consequently affect the measurement of some observables. [1]

In this report, we focus on the semileptonic exclusive decay $B \to K^*\ell^+\ell^-$.

2 Theoretical framework

Rare B decays are challenging due to the multiple physical scales involved. FCNCs are a multi-scale problem. The heavier scale is the electroweak one, $M_W \simeq 80\,\text{GeV}$, that is set by the heavy particle exchange in the loop. The scale set by the external particles is $m_b \simeq 4\,\text{GeV}$, while the hadrons dynamics is characterised by $\Lambda_{QCD} \simeq 0.2GeV$ (where QCD is non-perturbative). Hence, there is a large energy gap $M_W \gg m_b \gg \Lambda_{\text{QCD}}$ [2]. Therefore, effective field theory (EFT) methods can help us to deal with this multi-scale problem.
At dimension 6, the effective Hamiltonian for $b \to s\ell^+\ell^-$ transitions can be written as [3]

$$\mathcal{H}_{eff} = \frac{-4G_F}{\sqrt{2}}\left[V_{tb}V_{ts}^* \sum_{i\neq 1u,2u} C_i(\mu)O_i(\mu) + h.c.\right] . \tag{2.1}$$

where G_F is the Fermi constant, V_{ij} denote the elements of the CKM matrix, C_i are the Wilson coefficients and O_i the effective operators. In the SM, semileptonic decays $b \to s\ell^+\ell^-$ are mediated by $O_{7,9,10}$:

$$\begin{aligned} O_7 &= \frac{e}{(4\pi)^2} m_b(\bar{s}_L\sigma^{\mu\nu}b_L)F_{\mu\nu} , \\ O_9 &= \frac{\alpha}{4\pi}(\bar{s}_L\gamma^\mu b_L)(\bar{\ell}\gamma_\mu\ell) , \\ O_{10} &= \frac{\alpha}{4\pi}(\bar{s}_L\gamma^\mu b_L)(\bar{\ell}\gamma_\mu\gamma_5\ell) \end{aligned} \tag{2.2}$$

where $\sigma_{\mu\nu} = \frac{i}{2}[\gamma_\mu, \gamma_\nu]$ and $F_{\mu\nu}$ is the field strength of the photon. In generic NP scenarios, we also have the additional operators $O'_{7,9,10}$, where we exchange left- with right-handed fields in the quark current.
In order to compute the branching ratio of $B \to K^*\ell^+\ell^-$, we need to

- Separate short-distance effects (QCD, weak interaction and NP) from long-distance QCD,
- Compute the hadronic matrix element for $B \to K^*$ in terms of the K^* transversity amplitudes,
- Write the hadronic matrix element for $B \to K\pi$ in terms of the K^* transversity amplitudes,

- Find the differential decay distribution for $B \to K\pi\ell^+\ell^-$,
- Integrate over the angles and find the total decay distribution,
- Integrate over the q^2 range we are interested in to find the branching ratio.

2.1 Form Factors

Given $q^\mu = p^\mu - k^\mu$, where p^μ and k^μ are the momenta of B and K^* respectively, the $B \to K^*$ matrix elements can be expressed in terms of eight form factors $A_{0,1,2,3}(q^2), V(q^2)$ and $T_{1,2,3}(q^2)$.

$$\begin{aligned}
\langle K^*|\bar{s}\gamma_\mu(1-\gamma_5)b|B\rangle &= -i\epsilon^*_\mu(m_B+m_{K^*})A_1(q^2) + ip_\mu(\epsilon^*_K\cdot q)\frac{2A_2(q^2)}{m_B+m_{K^*}} + \\
&+ iq_\mu(\epsilon^*_K\cdot q)\left\{\frac{2m_{K^*}}{q^2}(A_3(q^2)-A_0(q^2)) - \frac{A_2(q^2)}{m_B+m_{K^*}}\right\} - i\epsilon_{\mu\nu\rho\sigma}\epsilon^{*\nu}_K p^\rho q^\sigma\frac{2V(q^2)}{m_B+m_{K^*}}\,,\\
\langle K^*|\bar{s}\sigma^{\mu\nu}q_\nu(1+\gamma_5)b|B\rangle &= \epsilon^*_\mu T_2(q^2)(m_B^2-m_{K^*}^2) + (\epsilon^*\cdot q)p_\mu\left(2T_2(q^2)+T_3(q^2)\frac{q^2}{m_B^2-m_{K^*}^2}\right) + \\
&- (\epsilon^*\cdot q)q_\mu\left[T_2(q^2)+T_3(q^2)\frac{m_B^2-m_{K^*}^2+q^2}{m_B^2-m_{K^*}^2}\right] + i\epsilon_{\mu\nu\rho\sigma}\epsilon^{*\nu}p^\rho q^\sigma 2T_1(q^2)
\end{aligned} \tag{2.3}$$

where ϵ^*_μ is the polarisation vector of K^*. The form factor A_3 can be expressed as

$$A_3(q^2) = \frac{m_B+m_{K^*}}{2m_{K^*}}A_1(q^2) - \frac{m_B-m_{K^*}}{2m_{K^*}}A_2(q^2) \tag{2.4}$$

and remains with 7 independent form factors, where $A_0(0) = A_3(0)$ and $T_1(0) = T_2(0)$.

2.2 Transversity Amplitudes

It can be useful to express the hadronic matrix element in terms of the K^* transversity amplitudes $A_\perp, A_\parallel, A_0$ and A_t. First, the matrix element of the B meson decaying into an on-shell K^* and a virtual gauge boson with momentum q, which subsequently decays into a dilepton pair, can be computed as

$$M(B \to K^*V^*) = \epsilon^{*\mu}_K(m)H_{\mu\nu}L_\rho g^{\mu\rho} \tag{2.5}$$

where $\epsilon_K(m)$ is the polarisation vector of K^* with $m = 0, +, -$, $H_{\mu\nu}$ is the hadronic part of the squared amplitude and L_ρ is the leptonic one. Since V^* is a vector boson, it will have polarisation $n = 0, +, -$.
However, we will consider the subsequent $V^* \to \ell^+\ell^-$ decay, which introduces a fourth polarisation state $n = t$.
In the B–rest frame, $q^\mu = (E_q, 0, 0, p)$ and $k^\mu = (E_{K^*}, 0, 0, -p)$ and the polarisation vectors read

$$\begin{cases}
\epsilon^\mu_q(0) = \dfrac{(-p,0,0,-E_q)}{\sqrt{q^2}}\\[2ex]
\epsilon^\mu_q(\pm) = \dfrac{(0,1,\mp i,0)}{\sqrt{2}}\\[2ex]
\epsilon^\mu_q(t) = \dfrac{q^\mu}{\sqrt{q^2}}
\end{cases}
\qquad
\begin{cases}
\epsilon^\mu_{K^*}(0) = \dfrac{(-p,0,0,E_{K^*})}{m_{K^*}}\\[2ex]
\epsilon^\mu_{K^*}(\pm) = \dfrac{(0,1,\pm i,0)}{\sqrt{2}}
\end{cases}$$

and they satisfy the orthonormality and completeness relations

$$\epsilon_q^{*\mu}(n)\epsilon_{q,\mu}(n') = g_{nn'}, \qquad \sum_{n,n'} \epsilon_q^{*\mu}(n)\epsilon_q^{\nu}(n')g_{nn'} = g^{\mu\nu}. \tag{2.6}$$

By substituting these relations in eq.2.5 and introducing the helicity amplitudes H_m, for $m = 0,+,-$

$$H_m = M_{(m,m)}(B \to K^*V^*) = \epsilon_K^{*\mu}(m)\epsilon_q^{*\nu}(m)M_{\mu\nu} \tag{2.7}$$

we get

$$M(B \to K^*V^*) = \sum_n g_{nm}L_\rho\epsilon_q^\rho(n)H_m\,. \tag{2.8}$$

The transversity amplitudes are defined as

$$A_{\perp,\parallel} = (H_+ \mp H_-)/\sqrt{2}\,, \qquad A_0 = H_0 \tag{2.9}$$

and, since V^* is virtual, we also have an additional amplitude

$$A_t = M_{(0,t)}(B \to K^*q) \tag{2.10}$$

By contracting $\epsilon_{K^*}^{*\mu}H_{\mu\nu}$ and comparing the result with eq.2.3, we can find the explicit form of the 7 transversity amplitudes $A_\perp^{L,R}$, $A_\parallel^{L,R}$, $A_0^{L,R}$ and A_t [2]

$$\begin{aligned}
A_\perp^{L,R} &= N\sqrt{2}\sqrt{\lambda}\left[(C_9 \mp C_{10})\frac{V(q^2)}{m_B + m_{K^*}} + 2\frac{m_b}{q^2}C_7T_1(q^2)\right]\,,\\
A_\parallel^{L,R} &= -N\sqrt{2}\left[(C_9 \mp C_{10})(m_B + m_{K^*})A_1(q^2) + 2\frac{m_b}{q^2}(m_B^2 - m_{K^*}^2)C_7T_2(q^2)\right]\,,\\
A_0^{L,R} &= \frac{-N}{2m_{K^*}\sqrt{q^2}}\left\{(C_9 \mp C_{10})\left[(m_B^2 - m_{K^*}^2 - q^2)(m_B + m_{K^*}A_1(q^2) - \frac{\lambda}{m_B + m_{K^*}}A_2(q^2)\right] + \right.\,,\\
&\left.+2m_bC_7\left[(m_B^2 + 3m_{K^*}^2 - q^2)T_2(Q^2) - \frac{\lambda}{m_B^2 - m_{K^*}^2}T_3(q^2)\right]\right\}\,,\\
A_t &= 2N\sqrt{\frac{\lambda}{q^2}}C_{10}A_0(q^2)
\end{aligned} \tag{2.11}$$

where

$$\begin{aligned}
N &= V_{tb}V_{ts}^*\frac{G_F\,\alpha}{\sqrt{3\;2^{10}\pi^5m_B^3}}\sqrt{q^2}\sqrt{\beta}\lambda^{1/4}\,,\\
\beta &= \sqrt{1 - \frac{4m_\mu^2}{q^2}}\,,\\
\lambda &= m_B^4 + m_{K^*}^4 + q^4 - 2m_B^2q^2 - 2m_B^2m_{K^*}^2 - 2m_{K^*}^2q^2\,.
\end{aligned} \tag{2.12}$$

[2] L,R refer to the chirality of the leptonic current. Since $q_\mu(\bar{\ell}\gamma^\mu\ell) = 0$ from current conservation, A_t doesn't have separate components

2.3 Angular Coefficients

In experiments the actual observed decay is $B \to K^*(\to K\pi)\ell^+\ell^-$, which involves a 4-body decay amplitude, and the $B \to K\pi$ matrix element must be expressed in terms of the $B \to K^*$ form factors. From [4], the 4-body decay rate can be written as

$$d\Gamma = \frac{|\mathcal{M}|^2}{4(4\pi)^6 m_B^3}\frac{\sqrt{\lambda}}{2}\beta_K\beta_\ell dk^2 d\cos\theta_\ell d\cos\theta_{K^*} d\cos\phi dq^2 \tag{2.13}$$

where λ is defined as in eq.2.12, $\beta_K = \sqrt{1-\frac{4m_B^2}{k^2}}$, $\beta_\ell = \sqrt{1-\frac{4m_\ell^2}{q^2}}$, θ_ℓ is the angle of ℓ in q–rest frame w.r.t. q direction of flight and θ_{K^*} is the angle of π in K^*–rest frame w.r.t. K^* direction of flight and ϕ is the angle between $(K\pi)$–$(\bar{\ell}\ell)$ plane in B rest frame (see fig.2.1).

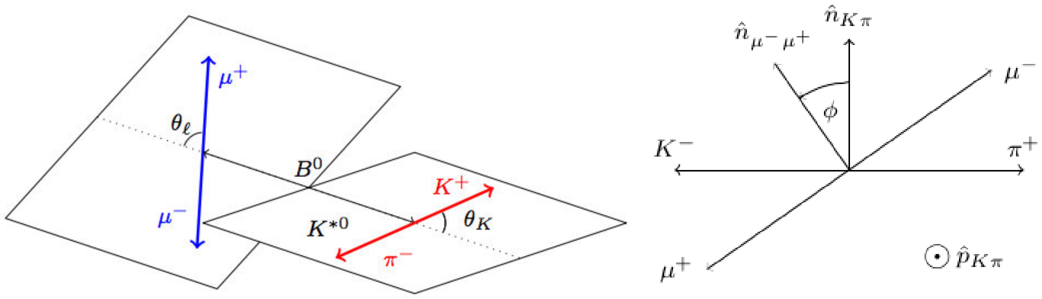

Figure 2.1: Graphical representation of the angular basis from [5]

Assuming that K^* decays resonantly, in the narrow width approximation we can replace in the squared K^* propagator

$$\frac{1}{(k^2 - m_{K^*}^2) + (m_{K^*}\Gamma_{K^*})^2} \xrightarrow{\Gamma_{K^*} << m_{K^*}} \frac{\pi}{m_{K^*}\Gamma_{K^*}}\delta(k^2 - m_{K^*}^2)\,. \tag{2.14}$$

If we use this and the transversity amplitudes we found before, the differential decay width becomes

$$\frac{d^4\Gamma}{dq^2 d\cos\theta_\ell d\cos\theta_{K^*} d\cos\phi} = \frac{9}{32\pi} I(q^2,\theta_\ell,\theta_{K^*},\phi) \tag{2.15}$$

where

$$\begin{aligned} I(q^2,\theta_\ell,\theta_{K^*},\phi) = {} & I_1^s \sin^2\theta_{K^*} + I_1^c \cos^2\theta_{K^*} + (I_2^s \sin^2\theta_{K^*} + I_2^c \cos^2\theta_{K^*})\cos 2\theta_\ell + \\ & + I_3 \sin^2\theta_{K^*}\sin^2\theta_\ell\cos 2\phi + I_4 \sin 2\theta_{K^*}\sin 2\theta_\ell\cos\phi - I_5\sin 2\theta_{K^*}\sin\theta_\ell\cos\phi + \\ & - (I_6^s \sin^2\theta_{K^*} + I_6^c\cos^2\theta_{K^*})\cos\theta_\ell + I_7\sin 2\theta_{K^*}\sin\theta_\ell\sin\phi - I_8\sin 2\theta_{K^*}\sin 2\theta_\ell\sin\phi + \\ & - I_9\sin^2\theta_{K^*}\sin^2\theta_\ell\sin 2\phi\,. \end{aligned} \tag{2.16}$$

Integrating the decay amplitude over $\cos\theta_\ell, \cos\theta_K \in [-1,1]$ and $\phi \in [0, 2\pi]$, we get

$$\frac{d^4\Gamma}{dq^2} = \frac{1}{4}(3I_1^c + 6I_1^s - I_2^c - 2I_2^s) \tag{2.17}$$

where $I_{1,2}^{c,s}$ are non-trivial functions of the transversity amplitudes

$$\begin{aligned} I_1^c &= |A_0^L|^2 + |A_0^R|^2 + \frac{4m^2}{q^2}\left(|A_t|^2 + 2\,\mathrm{Re}(A_0^L A_0^{*R})\right) , \\ I_1^s &= \frac{2+\beta_\ell^2}{4}\left(|A_\parallel^L|^2 + |A_\parallel^R|^2 + |A_\perp^L|^2 + |A_\perp^R|^2\right) + \frac{4m^2}{q^2}\mathrm{Re}\left(A_\parallel^L A_\parallel^{*R} + A_\perp^L A_\perp^{*R}\right) , \\ I_2^c &= -\beta_\ell^2\left(|A_0^L|^2 + |A_0^R|^2\right) , \\ I_2^s &= \frac{\beta_\ell^2}{4}\left(|A_\perp^L|^2 + |A_\perp^R|^2 + |A_\parallel^L|^2 + |A_\parallel^R|^2\right) . \end{aligned} \tag{2.18}$$

2.4 Branching Ratio

If we integrate eq.2.17 over $q^2 \in [1.1, 6]\,\mathrm{GeV}^2$ that we find the theoretical prediction for the branching ratio in the bin of interest.
Since we are dealing with rare decays, it is essential to consider the theoretical uncertainties of the $B \to K^*$ form factors and the correlations among them [6]. We can introduce the complex variable

$$z(t) = \frac{\sqrt{t_+ - t_0} - \sqrt{t_+ - t}}{\sqrt{t_+ - t_0} + \sqrt{t_+ - t}} \tag{2.19}$$

where $t_+ = (m_B + m_{K^*})^2$, $t_0 = (m_B - m_{K^*})^2$, $t = q^2$, and write the seven form factors F_i as

$$F_i(z) = P_i(q^2)\sum_{k=0}^{\infty} \alpha_k^i \left[z(q^2) - z(0)\right]^k \tag{2.20}$$

where $P_i(q^2) = (1 - \frac{q^2}{m_{R,i}^2})^{-1}$ is a simple pole corresponding to the first resonance in the spectrum

F_i	A_0	T_1, V	T_2, T_3, A_1, A_3
$m_{R,i}$ [GeV]	5.366	5.415	5.829

Since $|z|^2 \leq 0.1$ for $B \to K^*$ and $\sum_k |a_k|^2 \leq 1$, the series can be truncated at z^2 and there will be three fit parameters for each of the seven F_i. Exploiting the relations $A_0(0) = A_3(0)$ and $T_1(0) = T_2(0)$, we can reduce the number of independent fit parameters from 21 to 19. Using these results[3], we can compute the error as

$$\sigma^2(BR) = \sum_{i,j} \frac{\partial BR}{\partial \alpha_i}\,\mathrm{Cov}(i,j)\,\frac{\partial BR}{\partial \alpha_j} . \tag{2.21}$$

The theoretical predictions of the branching ratio for different lepton families are

ℓ	$BR \cdot 10^{-7}$	$BR[1.1, 6] \cdot 10^{-7}\mathrm{GeV}^{-2}$
e	2.43 ± 0.30	0.50 ± 0.06
μ	2.42 ± 0.30	0.49 ± 0.06

Table 2.1: Branching ratios and differential branching ratios in bin $q^2 \in [1.1, 6]\mathrm{GeV}^2$

where

$$BR[q^2_{min}, q^2_{max}] = \frac{1}{q^2_{max} - q^2_{min}}\int_{q^2_{min}}^{q^2_{max}} \frac{dBR}{dq^2}dq^2 . \tag{2.22}$$

[3]See ancillary file "BKstar_LCSR-Lattice.json" of [6] for the $\alpha^i_{0,1,2}$ parameters and their correlation matrices

2.5 Comparison with Experimental Results

2.5.1 LHCb

If we compare the theoretical prediction for $\ell = \mu$ with the experimental result from the LHCb experiment [7]

$$BR_{th}[1.1, 6] = (0.494 \pm 0.062) \cdot 10^{-7} GeV^{-2}\,,$$
$$BR_{LHCb}[1.1, 6] = (0.342^{+0.017}_{-0.017} \pm 0.009 \pm 0.023) \cdot 10^{-7} GeV^{-2}$$

where the first experimental uncertainty is statistical, the second systematic and the third due to the uncertainty on the $B^0 \to J/\psi K^*$ and $J/\psi \to \mu^+\mu^-$ branching fractions.

We notice that there is a discrepancy. This difference can be attributed to two possible explanations. The first possibility is the existence of new physics beyond the Standard Model, that would modify the Wilson coefficient C_9 such that $C_9^{new} = C_9^{SM} + C_P^{NP}$, where C_9^{SM} represents the Standard Model contribution and C_p^{NP} the new physics one. The second possibility is that the effects of charm loops, which have not been considered so far, play a significant role.

In either scenarios, we can compute the BR keeping C_9 as a free parameter and minimize

$$\chi^2 = \frac{(BR_{LHCb} - BR_{SM+NP}(C_9))^2}{\sigma^2_{LHCb} + \sigma^2_{SM+NP}} \tag{2.23}$$

finding

$$C_9^{new} = 1.97 \pm 1.79\,.$$

In order to quantify the deviation from the Standard Model, we can compare this result with $C_9^{SM} = 4.273 \pm 0.251$ [8]

$$\Delta C_9^{LHCb} = \frac{C_9^{SM} - C_9^{new}}{\sqrt{\sigma^2_{SM} + \sigma^2_{new}}} = 1.295 \pm 0.990\,. \tag{2.24}$$

2.5.2 ATLAS

Since the ATLAS collaboration has started studies on rare decays such as $B \to K^*(892)\ell^+\ell^-$, we can apply a similar analysis to the one performed for the LHCb data. Given that ATLAS anticipates an experimental uncertainty of approximately 25% in the muon channel, we assume that the branching ratio for this decay will be consistent with that measured by LHCb. Under this assumption, the expected differential branching ratio is

$$dBR_{ATLAS}/dq^2 = (0.342 \pm 0.086) \cdot 10^{-7} GeV^{-2}\,.$$

Using this estimate, we perform a fit for the Wilson coefficient C_9 and find

$$C_9^{new} = 1.97 \pm 2.74$$

with deviation from the Standard Model prediction

$$\Delta C_9^{ATLAS} = 0.848 \pm 0.996\,. \tag{2.25}$$

While the precision of the ATLAS measurement is expected to be lower than that of LHCb due to the larger uncertainty, it remains a valuable independent probe of potential new physics contributions to the $B \to K^*(892)\ell^+\ell^-$ decay process.

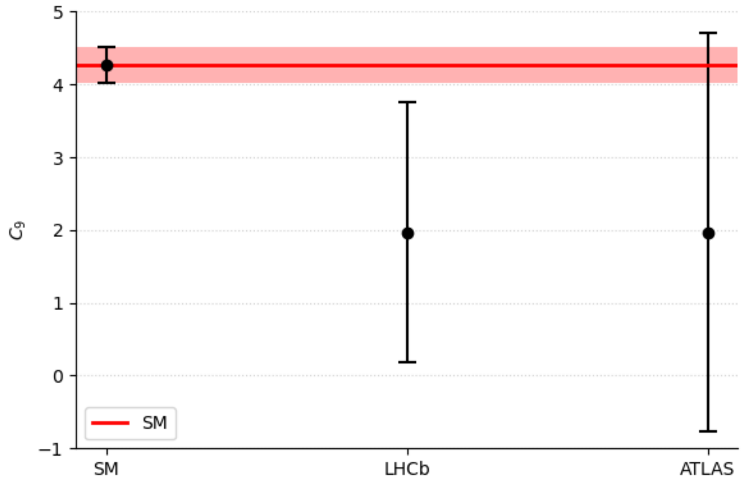

	C_9
SM	4.273 ± 0.251
LHCb	1.97 ± 1.79
ATLAS	1.97 ± 2.74

Figure 2.2: Comparison of extracted C_9 values

Although the observed discrepancies are intriguing, they are not yet conclusive evidence for new physics. Future research efforts in this area could focus on several key approaches:

- Improving the treatment of charm loop effects;
- Including the contribution of the resonances;
- Extending the analysis to other q^2 ranges;
- Incorporating data from other experiments and decay channels to perform global fits;
- Awaiting more precise measurements from LHCb and ATLAS to clarify the significance of these discrepancies.

3 S–wave Fraction Extraction

Using data from pp collision recorded by the ATLAS detector at $\sqrt{s} = 11$ TeV in 2018, we study the resonant decay $B^0 \to K^*(892) J/\psi(\to \ell^+\ell^-)$ in order to determine the S–wave fraction of the $K^+\pi^-$ system. The K^* decay products can be found in P–wave ($B^0 \to K^+\pi^- J/\psi$) or S–wave ($B^0 \to K^* J/\psi$) states.

3.1 Fit Studies for Signal Modelling

To determine the signal shape, we analyze Monte Carlo(MC) signal samples $B^0 \to J/\psi K^*$ (P–wave) and $J/\psi K\pi$ (S-wave). First, the fits are performed separately for the B^0 mass and the K^* mass to determine their individual shapes in the S– and P–wave components. Subsequently, a two-dimensional (2D) fit of both masses is performed to extract the S–wave fraction.

3.1.1 B^0 mass Fit

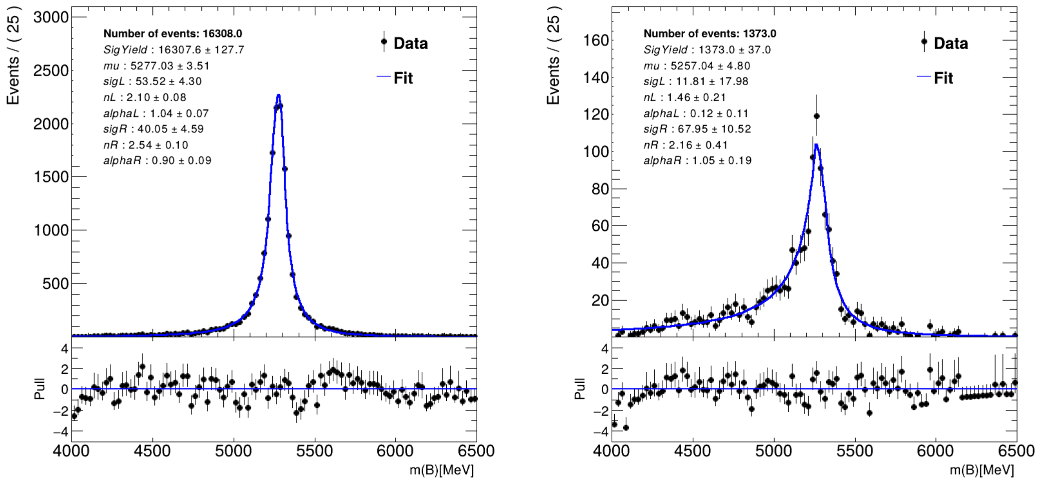

(a) P wave: Double Crystal Ball (DCB)

(b) S wave: DCB

Figure 3.1: B^0 mass Fit on MC signal samples

3.1.2 K^* mass Fit

Due to the inability of the ATLAS detector to distinguish between kaon and pion tracks, each set of four tracks corresponds two mass hypotheses: $B^0 \to K^+\pi^-\ell^+\ell^-$ or $\bar{B}^0 \to \pi^+K^-\ell^+\ell^-$. In order to select the best candidate between πK and $K\pi$ (where the first meson has positive charge and the second one negative), we used two algorithms

- Best πK: selects the best mass hypothesis based on the track information,
- Selected πK:if $K\pi$ is outside the baseline selection ($K\pi = -999$) selects πK, if $\pi K = -999$ selected $K\pi$, if both are valid, a random selection is made.

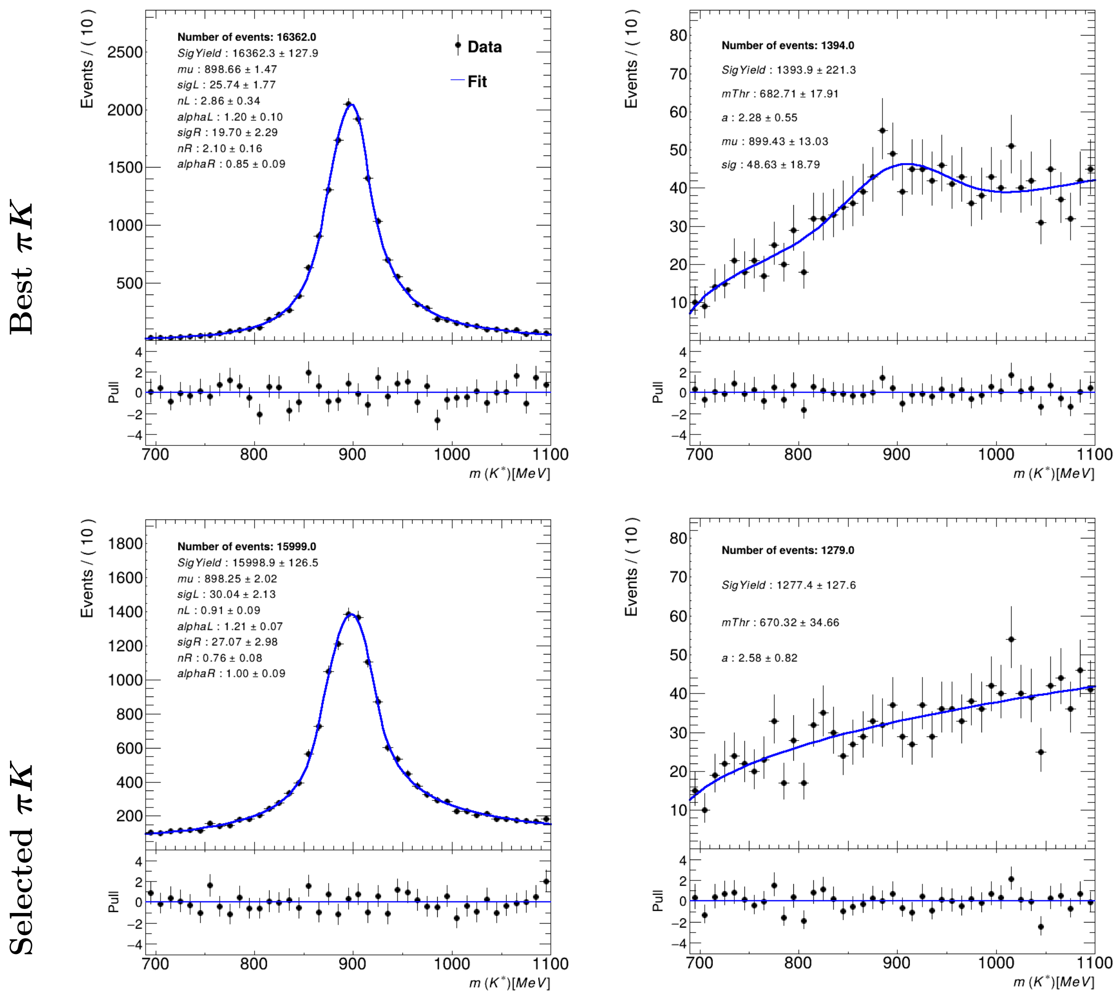

(a) P wave: DCB

(b) S wave: $(m_{Thr} - m_{K^*})^{1/a}$ [7]

Figure 3.2: K^* mass Fits on MC signal samples

3.1.3 2D Fit

The 2D distribution of the B^0 mass as a function of the K^* one is presented in fig.3.3. They can be considered uncorrelated, therefore the product of S– and P–wave PDFs can be used.

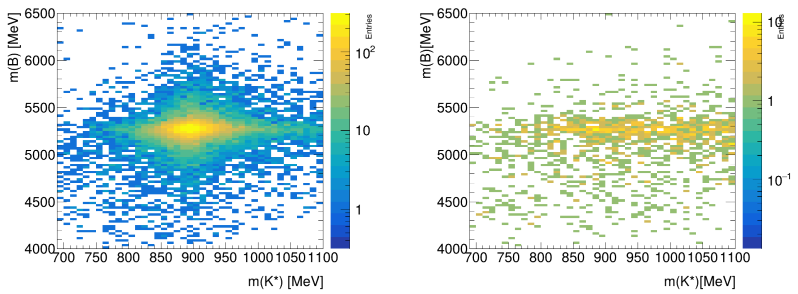

(a) P wave

(b) S wave

Figure 3.3: 2D Plot of B^0 mass vs Best K^* mass

Merging the two MC signal samples and using the shapes previously determined, a 2D simultaneous fit of B^0 and K^* masses was performed, first fixing K^* parameters in both waves, then fixing both B^0 and K^* parameters only in S–wave.

Figure 3.4: 2d Fit on MC signal samples–Best πK

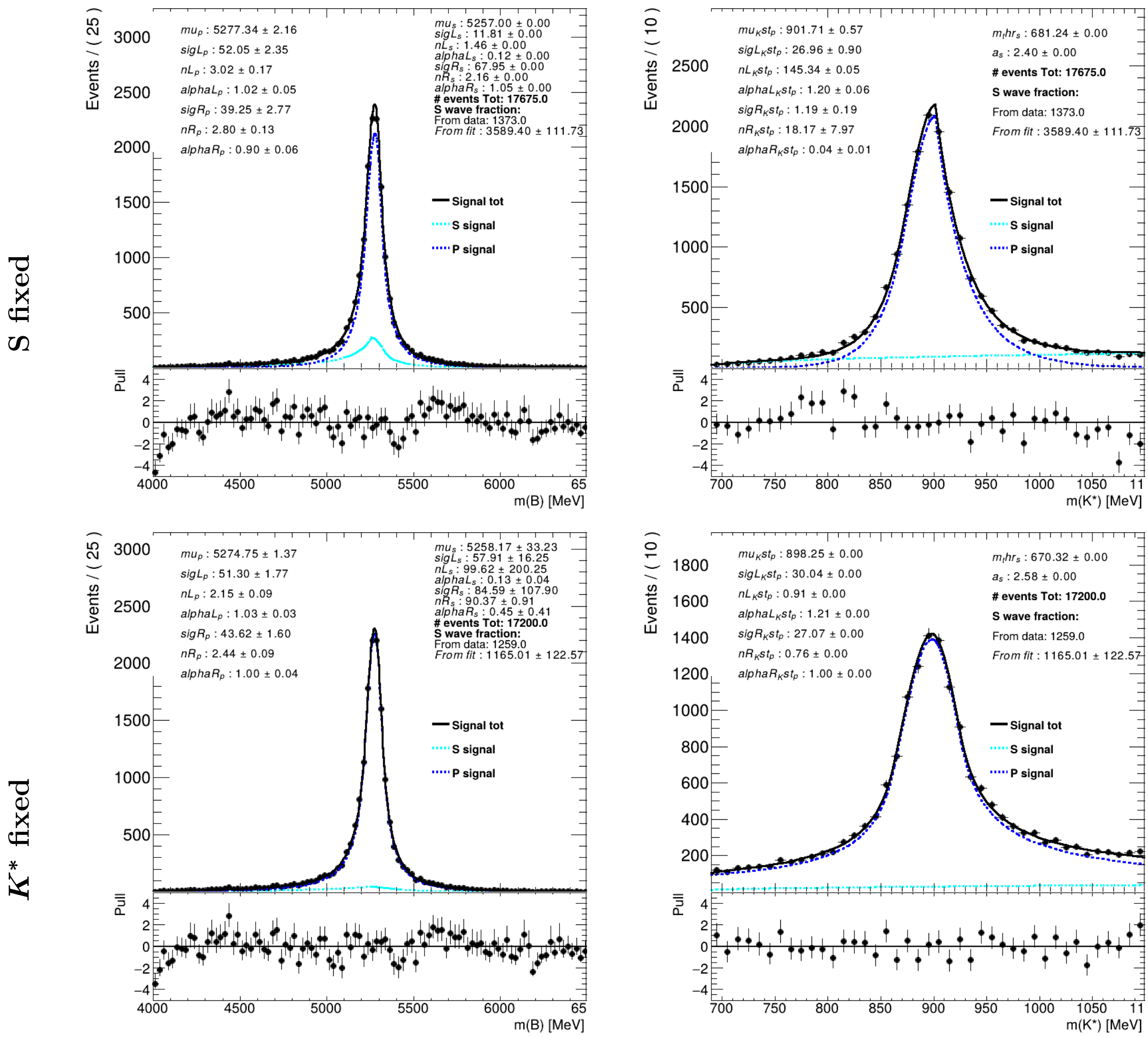

(a) B^0 mass

(b) K^* mass

Table 3.1: 2D Fit Results–Best πK

	K^* fixed		S fixed	
	# of events	Fit Yield	# of events	Fit Yield
Tot	17675	17675.06	17675	17675.06
P wave/channel	16302	15902 ± 141	16302	14086 ± 151
S wave/channel	1373	1773 ± 75	1373	3589 ± 112
S fraction	0.08	0.10	0.08	0.20

Figure 3.5: 2D Fit on MC signal samples–Selected πK

S fixed

K^* fixed

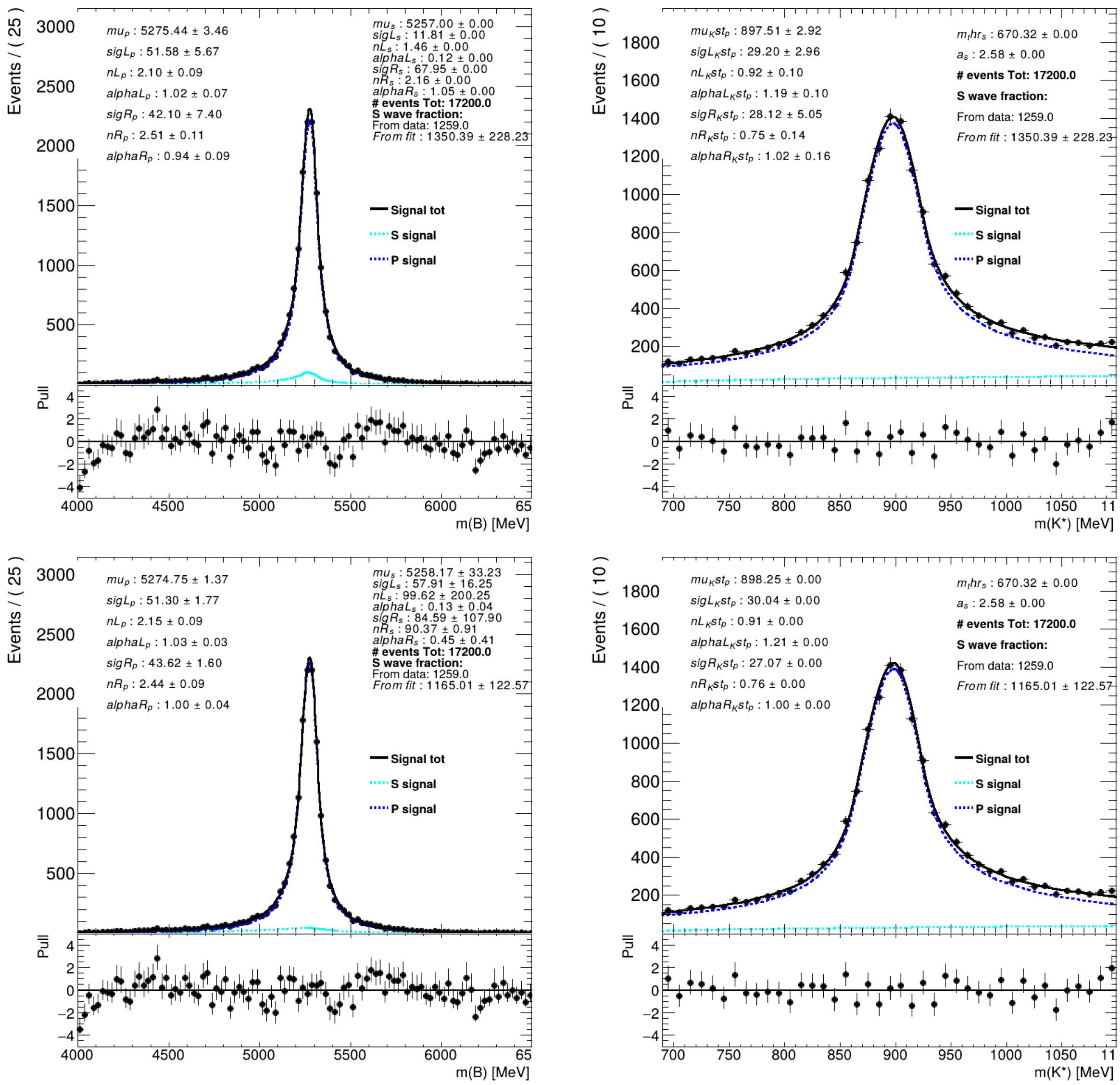

(a) B^0 mass

(b) K^* mass

Table 3.2: 2D Fit Results–Selected πK

	K^* fixed		S fixed	
	# of events	Fit Yield	# of events	Fit Yield
Tot	17200	17200.2	17200	17201.1
P wave	15941	16035 ± 169	15941	15851 ± 258
S wave	1259	1165 ± 123	1259	1350 ± 228
S fraction	0.073	0.067	0.073	0.078

3.2 Fit Studies for Background Modelling

3.2.1 K^* mass background

For the K^* mass background, I studied the Same Sign mesons data and the Low & High B^0 mass side-bands of the $J/\psi K^*$ resonant data:

- Low side-band: $m_B \in [4000, 4700]MeV$,
- High side-band: $m_B \in [5700, 6500]MeV$.

In both cases I applied the ϕ veto, that filters the data excluding $m_{KK} \in [1001.09, 1038.49]MeV$.

Best πK

Selected πK

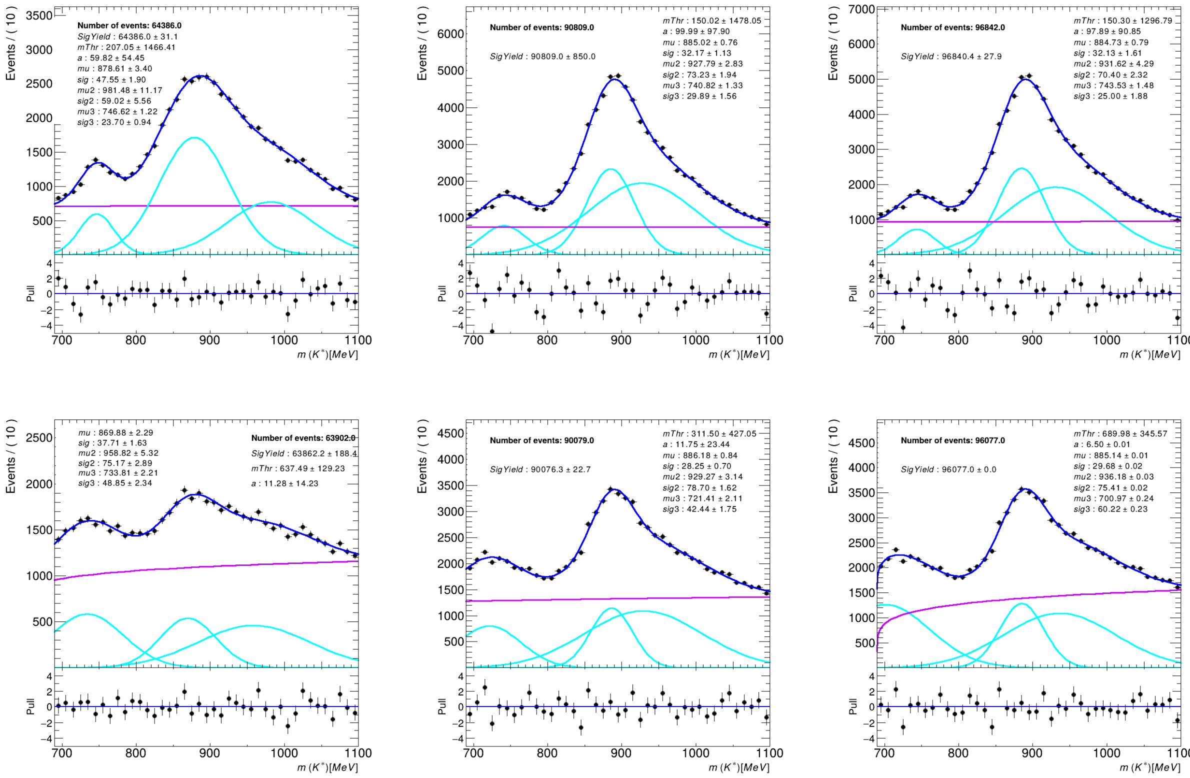

(a) Same Sign (b) Low sideband (c) Low+High sidebands

Figure 3.6: Same Sign vs $J/\psi K^*$ B^0 mass sidebands Fit

After comparing them, I chose to model the background with the shape of the side-bands, beacsue these are the events we have in our full fit as well.

3.2.2 B^0 mass background

For the B^0 mass, the background shape was determined doing a 1D fit of the data, using the shapes from the Monte Carlo to model the signal and a double crystal ball for the $J/\psi K^\pm$ resonance, as in fig.3.7, where the shape of the S–wave and the one of the $J/\psi K^\pm$ are fixed as shown in tab.3.3.

Table 3.3: S wave and $J/\psi K^{\pm}$ shapes

	μ	σ_L	α_L	n_L	σ_R	α_R	n_R
S wave	5257.04	11.81	0.12	1.46	67.95	1.05	2.16
$J/\psi K^{\pm}$	5427.1	12	0.22	2.15	84	0.56	4.2

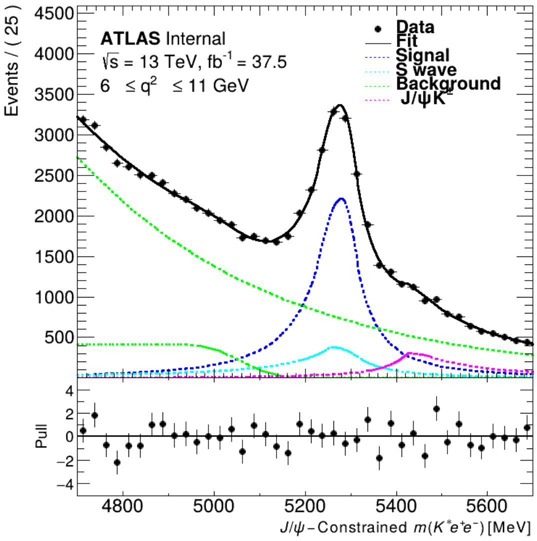

Figure 3.7: B^0 mass fit on 2018 data

	Fit param	Error
S Yield	7410	2398
P Yield	20515	724
μ	5280.87	1.02
σ_L	54.99	7.93
α_L	0.94	1.12
n_L	2.99	1.46
σ_R	35.25	5.02
α_R	0.89	0.35
n_R	2.01	0.99
Bkgr Yield	52006	884
μ_{Erf}	5061.97	12.84
k_{Erf}	2.64	0.71
λ_{Exp}	-0.00227	0.00006
$f_{Exp/Erf}$	0.88	0.01
$J/\psi K^{\pm}$ Yield	2951	94
# of Events	72521	–

3.3 2D Fit of B^0 and K^* mass

Using the shapes previously determined, a 2D simultaneous fit of the B^0 and K^* masses was performed on the $J/\psi K^*$ resonant data.

3.4 Best πK

	B^0 mass	K^* mass	Extracted Yield	Err
P wave	DCB fixed from MC	DCB fixed from MC	14428	1239
S wave	DCB fixed from MC	LHCb fixed from MC	1969	1571
Background	Exp+ErF fixed from data	LHCb + 3 Gauss fixed from sidebands	52761	323
$J/\psi K^{\pm}$ resonance	DCB fixed	–	3301	205

The S–wave fraction was then extracted from this fit, as shown in tab.3.4

Table 3.4: S wave fraction–Best πK

S Yield	Tot Signal Yield	% S
1969 ± 1571	16397 ± 2000	0.12 ± 0.09

Figure 3.8: 2D fit of B^0 vs K^* mass in two different ranges of m_{K^*}

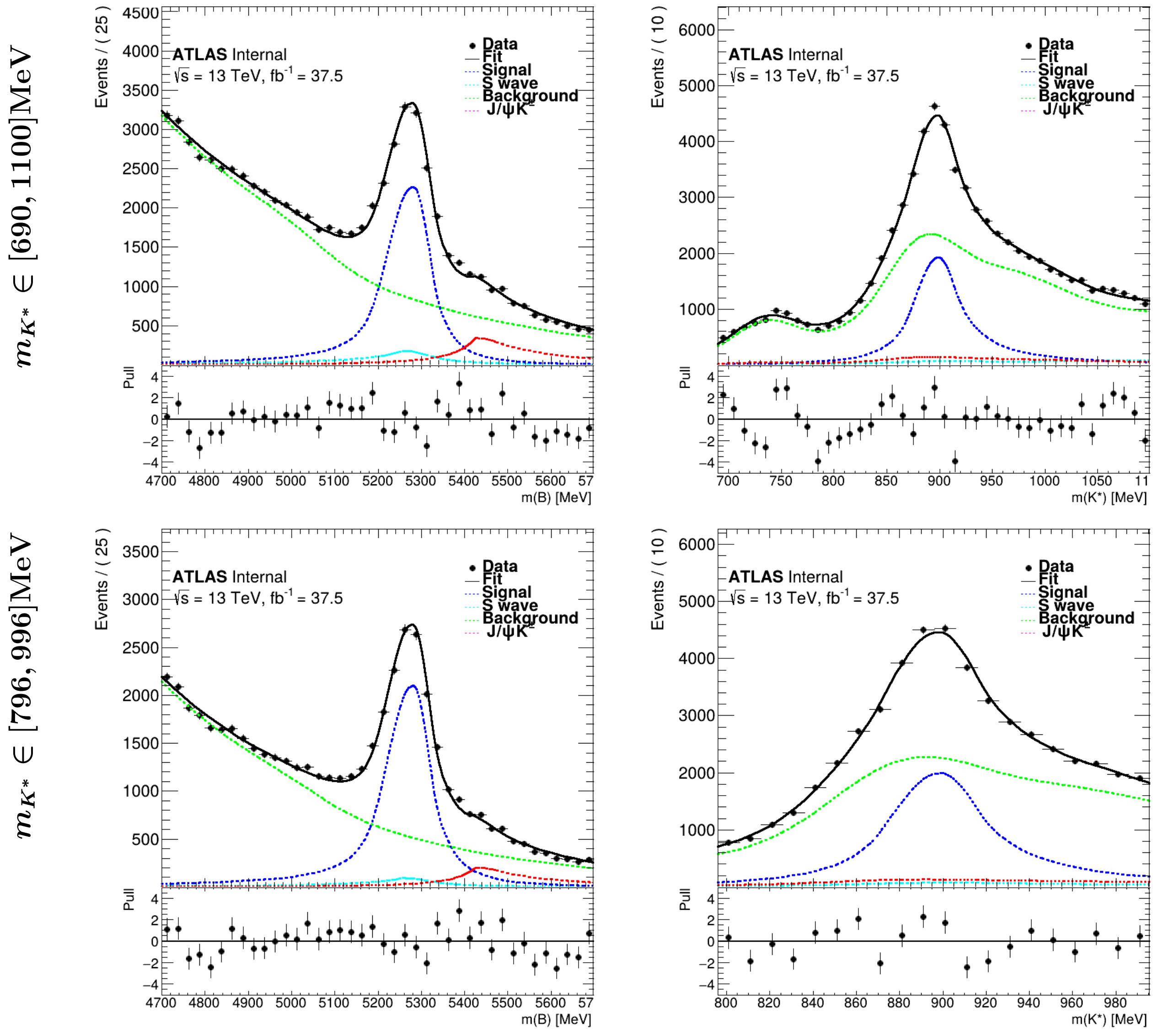

(a) B^0 mass

(b) K^* mass

Similarly, a restricted 2D fit in $m_{K^*} \in [796, 996]$MeV was performed.

	Extracted Yield	Err
P wave	13723	250
S wave	1024	304
Background	33346	296
$J/\psi K^{\pm}$ resonance	1936	142

Table 3.5: S wave fraction–Best πK restricted range

S Yield	Tot Signal Yield	% S
1024 ± 304	1474 ± 393	0.069 ± 0.021

3.4.1 Selected πK

The same analysis was performed using the *Selected* πK for m_{K^*}.

Figure 3.9: 2D fit of B^0 vs K^*–Selected πK

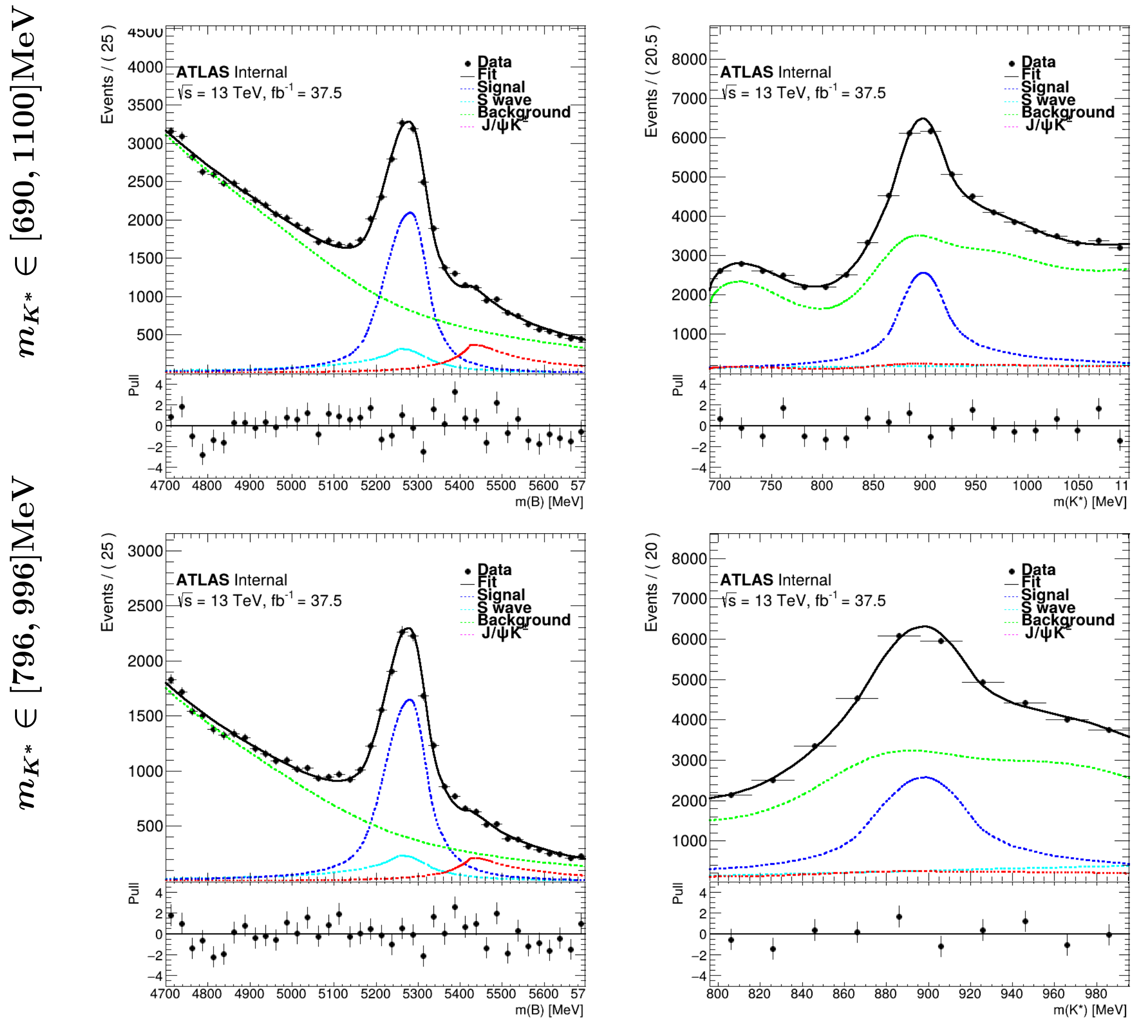

(a) B^0 mass

(b) K^* mass

	$m_{K^*} \in [690, 1100]$MeV		$m_{K^*} \in [796, 996]$MeV	
	Extracted Yield	Err	Extracted Yield	Err
P wave	12815	529	10384	459
S wave	3502	578	2598	543
Background	52059	681	26634	591
$J/\psi K^{\pm}$ resonance	3577	439	2044	279

Table 3.6: S wave fraction–Selected πK

m_{K^*}	S Yield	Tot Signal Yield	% S
$[690, 1100]$MeV	3502 ± 578	16317 ± 784	0.21 ± 0.04
$[796, 996]$MeV	2598 ± 543	12982 ± 711	0.20 ± 0.04

4 Conclusion

This comprehensive study of the decay $B^0 \to K^*\ell^+\ell^-$ has provided valuable insights into both the theoretical aspects and experimental measurements of this rare process, which serves as a sensitive probe for physics beyond the Standard Model.
In the theoretical analysis, we:

1. Derived a detailed framework for calculating the branching ratio, encompassing the effective Hamiltonian, form factors, transversity amplitudes, and angular coefficients.

2. Predicted branching ratios for electron and muon channels in the range $q^2 \in [1.1, 6]\,\mathrm{GeV}^2$, incorporating state-of-the-art form factor calculations and theoretical uncertainties.

3. Identified a notable discrepancy between our theoretical predictions and LHCb experimental results, potentially indicating new physics effects or underestimated charm loop contributions.

4. Quantified the deviation from the Standard Model by treating the Wilson coefficient C_9 as a free parameter, finding $\Delta C_9^{LHCb} = 1.295$ and anticipating $\Delta C_9^{ATLAS} = 0.848$.

Complementing this theoretical work, our experimental analysis using 2018 ATLAS data focused on extracting the S-wave fraction of the $K\pi$ system. We

1. Analyzed MC signal samples in order to find the shape of the signal.

2. Successfully modelled the background studying the same sign and $J/\psi K^*\, B^0$ mass side–bands.

3. Successfully extracted the S-wave fraction using both Best and Selected πK methods:

   - For $m_{K^*} \in [690, 1100]$ MeV, we found an S-wave fraction of $(12 \pm 9)\%$ and $(21 \pm 4)\%$ respectively.
   - For $m_{K^*} \in [796, 996]$MeV, we obtained $(6.9 \pm 2.1)\%$ and $(20 \pm 4)\%$ respectivey.

These results underscore the complexity of $B^0 \to K^*\ell^+\ell^-$ decays and their potential for probing new physics. The non-negligible S-wave component highlights the intricate dynamics of the $K\pi$ system, which must be considered in future analyses of rare B-meson decays involving vector mesons. Future directions for this research could include:

- Expanding the theoretical analysis to more q^2 bin;

- Refining our theoretical calculations to include resonances and charm loops effects;

- Extending the experimental analysis to all the data recorded by ATLAS during Run 2;

- Improving background modeling techniques to further reduce systematic uncertainties.

In conclusion, the study of $B^0 \to K^*\ell^+\ell^-$ continues to be a rich field for probing the limits of the Standard Model and searching for new physics. Our combined theoretical and experimental approach has provided valuable insights into the decay dynamics and potential new physics contributions. As experimental precision improves and theoretical uncertainties are reduced, this decay mode will remain at the forefront of flavor physics research, offering exciting prospects for future discoveries.

References

[1] T. Blake, G. Lanfranchi, and D. M. Straub, "Rare B decays as tests of the standard model," *Progress in Particle and Nuclear Physics* **92** (Jan., 2017) 50–91. `http://dx.doi.org/10.1016/j.ppnp.2016.10.001`.

[2] W. Altmannshofer, P. Ball, A. Bharucha, A. J. Buras, D. M. Straub, and M. Wick, "Symmetries and asymmetries of $B \to K^*\mu^+\mu^-$ decays in the standard model and beyond," *Journal of High Energy Physics* **2009** no. 01, (Jan., 2009) 019–019. `http://dx.doi.org/10.1088/1126-6708/2009/01/019`.

[3] M. Bordone, *B-physics in the Standard Model and Beyond*. PhD thesis, Zurich U., 2018.

[4] C. Geng and Y. Hsiao, "Semileptonic $B^- \to p\bar{p}\ell^-\bar{\nu}_\ell$ decays," *Physics Letters B* **704** no. 5, (Oct., 2011) 495–498. `http://dx.doi.org/10.1016/j.physletb.2011.09.065`.

[5] **LHCb** Collaboration, R. Aaij *et al.*, "Differential branching fraction and angular analysis of the decay $B^0 \to K^{*0}\mu^+\mu^-$," *Journal of High Energy Physics* **2013** no. 8, (Aug., 2013) . `http://dx.doi.org/10.1007/JHEP08(2013)131`.

[6] A. Bharucha, D. M. Straub, and R. Zwicky, "$B \to V\ell^+\ell^-$ in the standard model from light-cone sum rules," *Journal of High Energy Physics* **2016** no. 8, (Aug., 2016) . `http://dx.doi.org/10.1007/JHEP08(2016)098`.

[7] **LHCb** Collaboration, R. Aaij *et al.*, "Measurements of the S-wave fraction in $B^0 \to K^+\pi^-\mu^+\mu^-$ decays and the $B^0 \to K^*(892)^0\mu^+\mu^-$ differential branching fraction," *Journal of High Energy Physics* **11** (Apr., 2016) 047. `https://doi.org/10.48550/arXiv.1606.04731`.

[8] M. Bordone, G. Isidori, S. Mächler, and A. Tinari, "Short- vs. long-distance physics in $B \to K^{(*)}\ell^+\ell^-$: a data-driven analysis," *Eur. Phys. J. C* **84** no. 5, (2024) 547, `arXiv:2401.18007`.